

# Bayesian Nonparametric Differential Analysis for Dependent Multigroup Data with Application to Colorectal Cancer DNA Methylation

Chiyu Gu\*

Department of Statistics, University of Missouri  
and

Veerabhadran Baladandayuthapani

Department of Biostatistics, University of Texas M.D. Anderson Cancer Center  
and

Jeffrey Morris

Department of Biostatistics, University of Texas M.D. Anderson Cancer Center  
and

Subharup Guha

Department of Statistics, University of Missouri

---

\*This work was supported by the National Science Foundation under Award DMS-1461948 to SG and Award DMS-1463233 to VB, and by the National Institutes of Health under Grant R01 CA160736 to VB. The work was partially supported by the National Science Foundation under Grant DMS-1127914 to the Statistical and Applied Mathematical Sciences Institute, RTP, North Carolina.

## Abstract

With recent advances in array-based and next-generation sequencing technologies, cancer datasets involve widely varying sizes and scales, measurement variables, and correlation structures. An overarching scientific goal in cancer research is the invention of general statistical techniques that can cleanly sift the signal from the noise in identifying genomic signatures of the disease across a set of experimental or biological conditions.

We propose *BayesDiff*, a nonparametric Bayesian approach based on a novel class of first order mixture models, called the Sticky Poisson-Dirichlet process or multicuisine restaurant franchise. The BayesDiff methodology flexibly utilizes information from all the measurements and adaptively accommodates any serial dependence in the data to perform simultaneous inferences on the variables.

The technique is applied to analyze the motivating DNA methylation colorectal cancer dataset, which displays both serial correlations and complex interaction patterns. In simulation studies, we demonstrate the effectiveness of the BayesDiff procedure relative to existing techniques for differential DNA methylation. Returning to the motivating dataset, we detect the genomic signature for four subtypes of colorectal cancer.

*Keywords:* Genomic signature; First order models; BayesDiff; Mixture models; Multicuisine restaurant franchise; Sticky Poisson-Dirichlet process

# 1 Introduction

Recent advances in array-based and next-generation sequencing (NGS) technologies have revolutionized biomedical research, especially in cancer. The rapid decline in the cost of genome technologies enables the measurement of genomic activity at a very detailed resolution and provides genome-wide information at the transcriptomic (e.g., gene/mRNA expression), genomic (e.g., copy number variation), epigenomic (e.g., methylation), and proteomic levels on matched patient or tissue samples (Hamid et al. (2009)). These datasets involve intrinsically different sizes and scales of high-throughput data, providing genome-wide, high-resolution information about the biology of cancer.

A common goal is the identification of differential genomic signatures between samples corresponding to different treatments or biological conditions, such as treatment arms, response to adjuvant chemotherapy, tumor subtypes, or cancer stages. Especially challenging is the high dimensionality of genomic markers such as genes and probes, usually in the hundreds of thousands, and the relatively small number of patient samples, usually no more than a few hundred. This is a “small n, large p” problem that results in unstable inferences due to collinearity. Additionally, there exist complex interaction patterns, such as signaling or functional pathway-based interactions for gene or protein expression data, and genomic or chromosomal location-based serial correlation for sequencing data. These interaction patterns significantly affect the identification of differential genomic signatures.

## 1.1 Differential DNA methylation in colorectal cancer

DNA methylation is a vitally important epigenetic mechanism that occurs by the addition of a methyl (CH<sub>3</sub>) group to DNA, resulting in the modification of the gene functions. This occurs almost exclusively at cytosine-phosphate-guanine (CpG) sites. Alterations in DNA methylation, for example, hypomethylation of oncogenes and hypermethylation of tumor suppressor genes (Feinberg & Tycko (2004)), are often associated with the development and

progression of cancer. It was previously believed that DNA methylation alterations almost exclusively occur in promoter regions or in CpG islands, which are chromosomal regions with a high frequency of CpG sites. However, it has been shown that the majority of methylation alterations in cancer do not occur in either promoters or CpG islands (Irizarry et al. (2009)). For these reasons, it is necessary to investigate DNA methylation alterations on a epigenome-wide basis.

Colorectal cancer is caused by the accumulation of genetic and epigenetic alterations in colonic epithelial cells during neoplastic transformation. It is one of the major cancers worldwide and the second death-causing cancer in the U.S. (Siegel et al. (2017)). Aberrant DNA methylation in the colon arises in tumor-adjacent mucosa that appears normal. This also contributes to later stages of colon carcinogenesis through simultaneous methylation in certain genes that alter specific oncogenic pathways (Kim et al. (2010)). Recently, Guinney et al. (2015) have proposed a comprehensive way to classify colorectal cancer into four consensus molecular subtypes (CMS). The identification of differentially methylated CpG sites on the epigenome is therefore key in understanding the biological mechanism and developing target treatments for the four subtypes of colorectal cancer.

The motivating dataset was obtained from a DNA methylation array experiment conducted at MD Anderson Cancer Center, Houston, Texas, on 163 samples obtained from patients with colorectal cancer. The data consist of DNA methylation levels for 485,577 probes. Each probe measures the methylation level at one CpG site. The samples are classified into 4 CMS subtypes; the methylation levels are in the form of percentage methylation values, ranging from 0 (no methylation) to 1 (maximum methylation).

The first panel of Figure 1 shows the methylation levels for a small portion of chromosome 11 on CpG sites near the gene NCAM1. The numerous subtle changes in the methylation levels of the samples suggest the need for sophisticated statistical analyses. In an exploratory investigation, we estimated the first order autocorrelations of neighboring sites and tested for overall significance. The results are shown in the second panel of Figure 1. The plot

reveals highly significant dependence between neighboring CpG sites, a common feature of DNA methylation datasets (Eckhardt et al. (2006); Irizarry et al. (2008); Leek et al. (2010)). The high variability of the inter-probe spacings suggests that distance-based dependencies would help more accurately model the data features.

**Existing statistical approaches.** Numerous frequentist and Bayesian methods have been developed for differential DNA methylation. Although a majority of the methods have been specifically designed for bisulfite sequencing data, some methods (e.g., IMA (Wang et al. 2012); COHCAP (Warden et al. 2013)) are applicable to DNA methylation arrays.

The existing approaches could be broadly classified into four categories: *(i) Testing-based methods*, such as IMA (Wang et al. 2012), COHCAP (Warden et al. 2013), and BSmooth (Hansen et al. 2012). These methods rely on two-sample or multiple-sample tests for the difference in means at each CpG site. *(ii) Regression based models*, such as methylkit (Akalin et al. 2012), bump hunting (Jaffe et al. 2012), Biseq (Hebestreit et al. 2013), and RADMeth (Dolzhenko & Smith 2014). After applying smoothing or other adjustments, these methods fit individual regression models for each CpG site and test for model significance. *(iii) Beta-binomial model-based methods*, such as MOABS (Sun et al. 2014), DSS (Feng et al. 2014), and methylSig (Park et al. 2014). These methods fit separate models based on the beta-binomial distribution at each CpG site and detect differential CpG sites via the estimated model parameters. *(iv) Hidden Markov models (HMMs)*, such as MethPipe (Song et al. 2013), Bisulfighter (Saito et al. 2014), and HMM-DM (Yu & Sun 2016). These methods rely on HMMs to model the methylation data for the entire genome and detect differentially methylated sites using the inferred hidden states.

The aforementioned methods have several shortcomings. For instance, most of the methods ignore the correlation of neighboring CpG sites. Non-HMM based methods construct separate models for each CpG site, resulting in low inferential accuracy due to small sample size. Beta-binomial, HMM, and most testing-based methods are able to accommodate

only two treatments or groups of samples. To handle multiple treatments, these techniques typically resort to low-power multiple comparison adjustments.

Among methods capable of accounting for serial dependence (e.g., HMMs), a common drawback is that they fail to adjust for the widely varying distances between CpG sites. That is, irrespective of the distances between adjacent CpG sites, these methods assume that the inter-site dependencies are uniform, even though there is strong empirical evidence that the dependencies decrease with increasing distance. The few methods that do account for inter-site distances (e.g., Hansen et al. 2012, Jaffe et al. 2012, Hebestreit et al. 2013) rely on ad hoc procedures to determine the bandwidths without incorporating the unique characteristics of individual datasets. Furthermore, the serial correlation in the methylation levels is often significantly weaker than that of the differential state categories of the CpG sites; the former condition implies the latter. Consequently, first order techniques that primarily model the correlations among the methylation levels may be suboptimal in applications. Finally, most existing methods are specially adapted to a particular data type (e.g., either DNA methylation arrays or bisulfite sequencing data), and cannot be generalized to differential analysis in datasets of different sizes and scales, e.g., gene or mRNA expression data.

This paper proposes general and flexible differential analysis methodology, not only for DNA methylation datasets, but for other types of transcriptomic, genomic, epigenomic, and proteomic data. We refer to the new approach as *BayesDiff*. The BayesDiff model is capable of adapting to the distinctive features of 'omics datasets. Instead of fitting a separate model for each gene or CpG site (generically, referred to as a “probe”), we impose a global model that accumulates the data from all  $p$  probes to make simultaneous inferences on the probes. A set of probe-specific, binary differential state variables delineates the genomic signature of the disease. These state variables are deterministic functions of a set of multivariate random effects.

To diminish the collinearity effects and achieve dimension reduction, we allocate the

probes to a smaller, unknown number of latent clusters based on the similarities in their multivariate random effects. Bayesian infinite mixture models are a natural choice for fitting an appropriate allocation mechanism. However, the existing mixture models in the literature have several disadvantages in differential analysis applications. For example, the degree of spatial dependence, when it exists, is independent of the inter-probe distances. Furthermore, the range of allocation patterns supported by these mixture models is often limited and may not sufficiently cover the common types of patterns observed in differential analysis applications.

We propose a novel extension of Poisson Dirichlet processes (PDPs) called the *Sticky PDP* or, equivalently, the *multicuisine restaurant franchise*. The new nonparametric stochastic process is capable of accommodating distance-based serial dependence between the probes. The strength of correlation is determined by a dependence parameter that is learned from the data. This enables the model to include between-probe correlations as part of the model structure and to flexibly adjust for different correlation strengths in a data-driven fashion. For example, it allows the spatial dependence to be 0. Furthermore, the model permits the dataset to direct the choice between PDPs, and their special case, Dirichlet processes, in detecting the best-fitting allocation pattern. We implement a fully Bayesian inferential procedure using a Markov chain Monte Carlo (MCMC) algorithm specially developed for posterior inferences in Sticky PDPs. Bayesian false discovery rate (FDR) control is considered in the posterior inference to adjust for multiplicity.

The rest of the paper is organized as follows. Section 2 describes the BayesDiff model and constructs the new stochastic process, the Sticky PDP or multicuisine restaurant franchise, on which the model relies. The MCMC algorithm and related inference procedures are outlined in Section 3. For various scenarios, Section 4 uses artificially generated datasets to evaluate the accuracy of BayesDiff in detecting disease genomic signatures. We show that our approach significantly outperforms existing methods for multigroup comparisons, not only in serially correlated datasets, but also in spatially uncorrelated data. We demonstrate

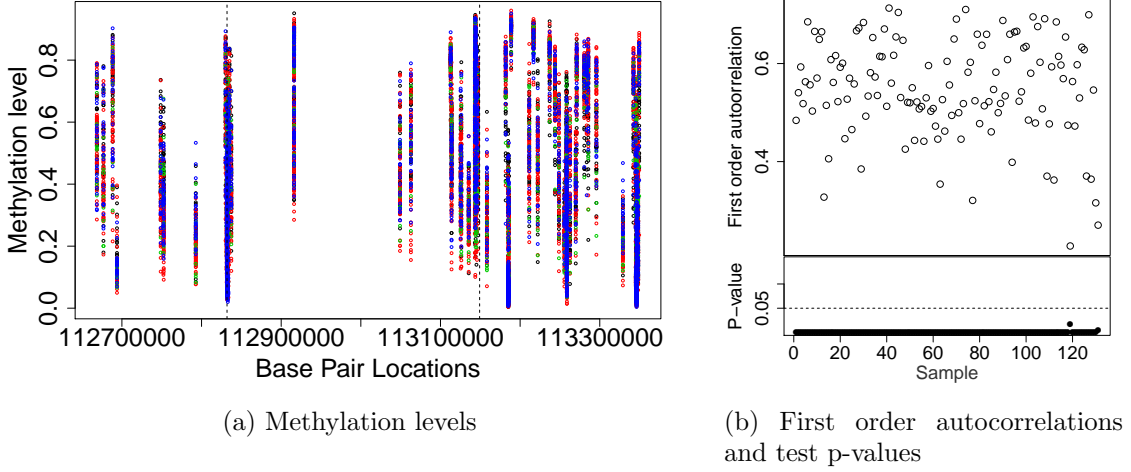


Figure 1: Exploratory analysis of the CpG sites near gene NCAM1 for the motivating colorectal cancer data. See the text for further explanation.

that our proposed model can correctly identify whether there is dependence and can detect the correct model structure. The motivating colorectal cancer dataset is analyzed by the BayesDiff procedure in Section 5. Conclusions and possible extensions to the BayesDiff approach are discussed in Section 6.

## 2 The BayesDiff Model

Imagine that we have continuous, proportion, or count measurements on  $p$  biomarkers, such as genes or CpG sites (“probes”), on  $n$  matched patient or tissue samples (“individuals”), with  $p$  being much larger than  $n$ . The data are arranged in an  $n \times p$  matrix,  $\mathbf{X} = ((x_{ij}))$ . Suppose the probes are sequentially indexed along a one-dimensional transcriptomic, genomic, epigenomic, or proteomic path. The distances between the adjacent probes along this path are denoted by  $e_1, \dots, e_{p-1}$ . These distances typically have significant variability due to the different spacings of the biomarkers.

Each individual  $i$  is associated with an experimental or biological condition (“treatment”)



with label  $t_i$  taking values in the set  $\{1, \dots, T\}$ , where  $T \geq 2$ . Let  $\xi_i$  represent the random effect of individual  $i$  and  $\theta_{tj}$  be the random effect associated with the treatment  $t$ -probe  $j$  combination. The primary analytical goal is the detection of probes whose treatment-specific effects are not all identical. These *differential probes* are said to constitute the genomic signature of the disease.

For a suitably chosen platform-specific transformation  $z(\cdot)$ , assume that

$$z_{ij} = z(x_{ij}) \sim N(\xi_i + \theta_{t_{ij}}, \sigma^2). \quad (1)$$

For count data  $x \in \mathbb{N}$ , an appropriate transformation may be  $z(x) = \log(1 + x)$ . For proportion data  $0 < x < 1$ , the logit function,  $z(x) = \log(x / (1 - x))$  may be appropriate. For continuous data  $x \in \mathbb{R}$ , we could simply choose the identity transformation.

Variance parameter  $\sigma^2$  in expression (1) is given an inverse gamma prior. We decompose parameter  $\xi_i$  into interpretable deterministic and stochastic components:

$$\xi_i = b_i + \epsilon_i, \quad (2)$$

where  $b_i$  is a known (possibly identically zero) individual-specific normalization constant and  $\epsilon_i$  represents the residual individual variability that is assumed to be iid normal:  $\epsilon_i \stackrel{iid}{\sim} N(0, \tau_\epsilon^2)$ . The resulting hyperparameter  $\tau_\epsilon^2$  is given an inverse-Gamma prior.

Inference focuses on features of the probe-specific vector of random effects,  $\boldsymbol{\theta}_j = (\theta_{1j}, \dots, \theta_{Tj})'$ , where  $j = 1, \dots, p$ . In particular, we define a binary *differential state variable*,  $s_j$ , with the value  $s_j = 1$  indicating that probe  $j$  is not differential, and the value  $s_j = 2$  indicating that it is differential. Applying the afore-mentioned notion of the disease genomic signature, we

have that

$$s_j = \begin{cases} 1 & \text{if } \theta_{1j} = \theta_{2j} = \dots = \theta_{Tj}, \\ 2 & \text{otherwise,} \end{cases} \quad (3)$$

for  $j = 1, \dots, p$ . The key parameters of interest are the differential state variables,  $s_1, \dots, s_p$ , and the disease genomic signature is the set of probes with state  $s_j = 2$ .

We assume flexible Bayesian nonparametric models for the random effects  $\boldsymbol{\theta}_1, \dots, \boldsymbol{\theta}_p$  of the probes. The details of these models are given below. Furthermore, the MCMC strategies of Section 3 are scalable to the ubiquitous big datasets in cancer research.

## Modeling the probe clusters

The analytical challenges posed by cancer data include not only high-dimensionality, but also dependencies between physically proximal probes and dependencies due to longer-range biological interactions between non-adjacent probes, for example, through signaling or functional pathway-based interactions. The dependencies result in multicollinearity in the matrix  $\mathbf{X}$  and cause inaccuracies in estimation and uncertainty quantification.

To mitigate the effects of collinearity and extract information from the large number of probes through dimension reduction, we allocate the  $p$  probes to a smaller number,  $q$ , of latent clusters, based on the similarities in their probe-specific random effects,  $\boldsymbol{\theta}_j$ . Suppose that allocation variable  $c_j$  assigns probe  $j$  to one of the  $q$  latent clusters. For  $j = 1, \dots, p$  and  $k = 1, \dots, q$ , variable  $c_j$  equals  $k$  if the  $j^{th}$  probe belongs to the  $k^{th}$  cluster.

Assume that the  $q$  clusters are respectively associated with  $T$ -variate *latent vectors*,  $\boldsymbol{\phi}_1, \dots, \boldsymbol{\phi}_q$ , and that the random effects and latent vectors are related as follows:

$$\boldsymbol{\theta}_j = \boldsymbol{\phi}_k \quad \text{if } c_j = k, \quad (4)$$

for probe  $j = 1, \dots, p$ , and cluster  $k = 1, \dots, q$ . Consequently, all probes assigned to a cluster have identical random effects equal to that cluster’s latent vector. The probes’ differential state variables, defined in equation (3), are therefore an attribute of the cluster. Clusters may be either differential or non-differential, and the condition  $\theta_{1j} = \theta_{2j} = \dots = \theta_{Tj}$  in equation (3) is then equivalent to

$$\phi_{1k} = \phi_{2k} = \dots = \phi_{Tk} \quad (5)$$

provided probe  $j$  belongs to cluster  $k$  (that is, provided  $c_j = k$ ). We define the set of *differential clusters* as

$$\mathcal{D} = \left\{ k : \phi_{tk} \neq \phi_{t'k}, \text{ for some } t \neq t', k = 1, \dots, q \right\}$$

**Mixture models for allocations.** Bayesian infinite mixture models are a natural choice for allocating  $p$  probes to a smaller, unknown number of latent clusters based on the similarities between the probes. Dirichlet processes Ferguson (1973) are the most frequently used infinite mixture models; see Müller & Mitra (2013, chap. 4) for a comprehensive review. The use of Dirichlet processes to achieve dimension reduction in high-dimensional settings has precedence in the literature; see Medvedovic et al. (2004), Kim et al. (2006), Dunson et al. (2008) and Dunson & Park (2008). Lijoi, Mena & Prünster (2007a) advocated the use of Gibbs-type priors (Gnedin & Pitman 2005, Lijoi, Mena & Prünster 2007b) for accommodating more flexible clustering mechanisms. In particular, (Lijoi et al. 2007a) demonstrated the utility of Poisson-Dirichlet processes (PDPs) in genomic applications. Guha & Baladandayuthapani (2016) introduced PDP-based clustering, variable selection, and prediction techniques for high-dimensional regression, demonstrating that PDPs are overwhelmingly favored to Dirichlet processes in benchmark cancer datasets. This is primarily because PDPs assign greater probability mass to allocation patterns with slow power law decay and large

numbers of small-sized clusters, a common characteristic of several cancer datasets.

The two-parameter PDP (Perman et al. (1992)) relies on a discount parameter,  $0 \leq d < 1$ , positive mass parameter,  $\alpha$ , and  $T$ -variate base distribution,  $W$ , and is denoted by  $\mathcal{W}(d, \alpha, W)$ . When  $d = 0$ , this yields a Dirichlet process with mass parameter  $\alpha$  and base distribution  $W$ . Suppose the sequence of random effects  $\theta_1, \dots, \theta_p$  have distribution  $\mathcal{W}(d, \alpha, W)$ . The *stick-breaking representation* of a PDP is  $\theta_j \stackrel{iid}{\sim} \mathcal{P}$ , where random distribution  $\mathcal{P}$  is the discrete mixture,  $\sum_{v=1}^{\infty} \pi_v 1_{\phi_v}$ , with  $1_{\phi_v}$  denoting a point mass at the atom  $\phi_v \stackrel{iid}{\sim} W$ . The random stick-breaking probabilities have the form:  $\pi_1 = V_1$  and  $\pi_h = V_h \prod_{v=1}^{h-1} (1 - V_v)$  for  $h > 1$ , where  $V_h \stackrel{indep}{\sim} \text{beta}(1 - d, \alpha + hd)$ .

Although the aforementioned techniques achieve dimension reduction in the large number of probes and account for long-range biological interactions between non-adjacent probes, a potential drawback is their implicit assumption of apriori probe exchangeability. Consequently, they are unable to provide an explanation for serial correlation, which is an increasingly common feature of NGS datasets as they approach single base pair resolution due to the rapidly declining costs of genome technologies. Infinite HMMs, such as the hierarchical Dirichlet process hidden Markov model (HDP-HMM) (Teh et al. 2006) and Sticky HDP-HMM (Fox et al. 2011) may be utilized to fill this gap. In these models, probe  $j$  has an associated *group* depending on the previous random effect,  $\theta_{j-1}$ . The group, in turn, determines the distribution of random effect  $\theta_j$ .

Although infinite HMMs are a step in the right direction, but they have some undesirable features in differential analysis applications. First, their degree of first order dependence is uniform, irrespective of the inter-probe distances. This is unrealistic in cancer datasets where the correlation between adjacent probes is found to typically decrease with distance. (Hansen et al. (2012); Jaffe et al. (2012); Hebestreit et al. (2013)) Second, the set of distinct random effects in infinite HMMs has a bijective mapping with the set of generative groups, which is therefore infinite. However, an exploratory analysis of the motivating colorectal cancer

DNA methylation dataset reveals that the serial correlation in ad hoc estimates of the  $p$  random effect vectors, although significant, is far weaker than the serial dependence between ad hoc estimates of the  $p$  binary state variables, defined in equation (3). This suggests that a hypothetical two-group, rather than an infinite-group Markov model such as HPD-HMM or Sticky HDP-HMM, would provide a much better fit for the data. Third, the range of allocation patterns supported by infinite HMMs is relatively limited. In particular, patterns such as power law decays in the cluster sizes and relatively large numbers of small-sized clusters, a common feature of cancer datasets, are assigned relatively small probabilities by infinite HMMs.

Because mixture models in the literature have one or more of the aforementioned disadvantages in differential analysis applications, we propose a novel extension of PDPs capable of accommodating distance-based serial dependence between the probes and allow fewer groups than random effects clusters. The model permits the dataset to direct the choice between PDPs and Dirichlet processes in detecting the best-fitting allocation pattern.

## 2.1 The Sticky PDP

Informally, a Sticky PDP consists of a cohort of regular PDPs generating a sequence of random effects  $\theta_1, \dots, \theta_p$  by a stochastic mechanism that switches generative PDPs at random locations along the sequence of probes. The formal definition is as follows:

Property 1: Set  $\mathcal{G}$  consists of a countable number of generative *groups*. Each group  $g \in \mathcal{G}$  comprises group-specific regular PDPs that are further indexed by an integer-valued *state* belonging to a countable set,  $\mathcal{S}$ . The bivariate PDP labels comprise the countable Cartesian product,  $\mathcal{G} \times \mathcal{S}$ .

Property 2: The regular PDPs may have equal or unequal discount parameters, mass parameters, and/or base distributions. For every index  $(g, s) \in \mathcal{G} \times \mathcal{S}$ , let the corresponding PDP

be  $\mathcal{W}_{gs}(d_s, \alpha_s, W_s)$ . Let a realization of the PDP's random stick-breaking distribution be denoted by  $\mathcal{P}_{gs}$ :

$$\begin{aligned} \mathcal{P}_{gs} &\stackrel{d}{=} \sum_{v=1}^{\infty} \pi_{gsv} \mathbf{1}_{\phi_{gsv}} \quad \text{where the atoms or latent vectors} \\ \phi_{gsv} &\stackrel{iid}{\sim} W_s, \quad v \geq 1, \text{ and the probabilities} \\ \pi_{gs1} &= V_{gs1}, \quad \pi_{gsh} = V_{gsh} \prod_{v=1}^{h-1} (1 - V_{gsv}), \quad h > 1, \quad \text{with} \\ V_{gsh} &\stackrel{indep}{\sim} \text{beta}(1 - d_s, \alpha_s + h d_s). \end{aligned} \tag{6}$$

If there are multiple states belonging to the set  $\mathcal{S}$ , assume that their base distributions  $\{W_s : s \in \mathcal{S}\}$  are such that two PDPs associated with unequal states have almost surely non-intersecting sets of atoms. That is, the intersection of the sets  $\{\phi_{g_1 s_1 v}\}_{v=1}^{\infty}$  and  $\{\phi_{g_2 s_2 v}\}_{v=1}^{\infty}$  is empty whenever  $s_1 \neq s_2$ .

Property 3: For probe  $j = 1, \dots, p$ , the label of the PDP that generates random effect  $\theta_j$  is denoted by  $(g_j, s_j) \in \mathcal{G} \times \mathcal{S}$ . Consequently,  $\theta_j \mid g_j, s_j \sim \mathcal{P}_{g_j s_j}$ . Equivalently, for the PDP cluster with label  $v_j$ , the random effect  $\theta_j$  is equal to  $\phi_{g_j s_j v_j}$  with PDP-specific probability  $\pi_{g_j s_j v_j}$ .

Property 4: Given the group  $g_j$  of the  $j^{th}$  probe, the state-specific PDP generating random effect  $\theta_j$  is selected as follows:

$$s_j \mid g_j \sim \mathcal{Q}_{g_j} \tag{7}$$

where, for every  $g \in \mathcal{G}$ ,  $\mathcal{Q}_g$  denotes a group-specific probability mass function on the set  $\mathcal{S}$ ; thus,  $\sum_{s \in \mathcal{S}} \mathcal{Q}_g(s) = 1$ .

Property 5: (*Markov property*) The group of the first probe,  $g_1$ , is random and marginally independent of the parameters of the downstream probes. For probe  $j > 1$ , given the

parameters associated with the previous probes, the group  $g_j$  has a mass function depending on random vector  $\boldsymbol{\theta}_{j-1}$  and inter-probe distance  $e_{j-1}$ :

$$g_j \sim \mathcal{F}_{\boldsymbol{\theta}_{j-1}, e_{j-1}} \quad (8)$$

where, for every  $\boldsymbol{\theta} \in \mathcal{R}^T$  and  $e > 0$ ,  $\mathcal{F}_{\boldsymbol{\theta}, e}$  denotes a probability mass function on the set  $\mathcal{G}$ , so that  $\sum_{g \in \mathcal{G}} \mathcal{F}_{\boldsymbol{\theta}, e}(g) = 1$ .

## 2.2 Multicuisine Restaurant Franchise

The Chinese restaurant franchise (CRF) metaphor for HDP-HMMs and Sticky HDP-HMMs (e.g., see Fox et al. 2011) can be generalized to the *multicuisine restaurant franchise* (MRF) to equivalently describe Sticky PDPs. The MRF comprises several restaurants (representing the groups) that are indexed by the set  $\mathcal{G}$ . Each restaurant is partitioned into separate sections (representing the states), with each section catering to a different cuisine indexed by the set  $\mathcal{S}$ . In the metaphor, regular PDPs, indexed by set  $\mathcal{G} \times \mathcal{S}$ , are represented by the restaurant-cuisine combinations.

A succession of customers arrive at times (representing the distances along a linear path)  $e_0, (e_0 + e_1), (e_0 + e_1 + e_2)$ , and so on. Every section in every restaurant has an infinite number of tables (representing PDP latent clusters) at which customers (representing the  $p$  random effects or probes) could potentially sit. All customers seated at a given table are served the same cuisine-specific dish (representing an atom or latent vector). Cuisines are uniquely identified by their dishes because no dish is shared by multiple cuisines.

At time  $e_0$ , Customer 1 randomly selects restaurant  $g_1$ , chooses cuisine  $s_1$  with restaurant-specific probability  $\mathcal{Q}_{g_1}(s_1)$ , and proceeds to the section serving that cuisine. Among the infinite tables in the section, Customer 1 chooses table  $v_1$  with cuisine-specific probability  $\pi_{g_1 s_1 v_1}$ , and is served the table-specific dish,  $\phi_{g_1 s_1 v_1}$ . The dish eaten by Customer 1 is then

recorded as  $\theta_1 = \phi_{g_1 s_1 v_1}$ .

After waiting time  $e_1$ , Customer 2 visits restaurant  $g_2 \sim \mathcal{F}_{\theta_1, e_1}$ , a random decision relying on the dish that the previous customer had eaten and on waiting time  $e_1$ . At restaurant  $g_2$ , Customer 2 chooses cuisine/section  $s_2$  with restaurant-specific probability  $\mathcal{Q}_{g_2}(s_2)$ . Customer 2 selects table  $v_2$  in this section with cuisine-specific probability  $\pi_{g_2 s_2 v_2}$ , and is served the table-specific dish,  $\phi_{g_2 s_2 v_2}$ . The outcome is recorded as  $\theta_2 = \phi_{g_2 s_2 v_2}$ . This process continues for subsequent customers. Although each restaurant offers all cuisines and serves every dish, the popularity of the cuisines, as well as the popularity of the dishes belonging to a cuisine, are both restaurant-specific.

In addition to extending PDPs to discrete time series type data, Sticky PDPs offer a diverse palette of parametric and nonparametric models for capturing the distinctive features of different datasets. The range of models includes Dirichlet processes, PDPs, infinite HMMs, hierarchical Dirichlet process (HDP) (Müller et al. (2004), Teh et al. (2006)), finite HMMs, nested Chinese restaurant processes (Blei & Jordan (2005)), nested Dirichlet processes (Rodriguez et al. (2008)), and analysis of densities models (Tomlinson & Escobar (2003)). Some examples are presented in Table 1. As suggested by the form of distribution  $\mathcal{F}_{\theta, e}$ , the first two examples in the table are first-order models and the remaining examples are zero-order models.

## 2.3 Sticky PDPs in Differential Analysis

We tailor Sticky PDPs to model the BayesDiff probe allocations. Adapting Properties 1–5 of Sections 2.1:

Property 1: The groups  $\mathcal{G}$  and states  $\mathcal{S}$  in the BayesDiff model are both equal to  $\{1, 2\}$ , with the set elements representing, respectively, non-differential and differential state. The four regular PDPs are indexed by  $(g, s) \in \{1, 2\} \times \{1, 2\}$  and are denoted by  $\mathcal{W}_{gs}(d_s, \alpha_s, W_s)$ .



Model	$\mathcal{G}$	$\mathcal{W}_{gs}(d_s, \alpha_s, W_s)$	$\mathcal{P}_g$	$\mathcal{F}_{\theta, e}$
HDP-HMM	$\mathcal{N}$	$\mathcal{W}_g(0, \alpha, W)$ , countably infinite $W$	$\sum_{v=1}^{\infty} \pi_{gv} \mathbf{1}_{\phi_v}$	Point mass at $\sum_{v=1}^{\infty} v \cdot \mathcal{I}(\theta = \phi_v)$
Finite HMM	$\{1, \dots, K\}$	$\mathcal{W}_g(0, \alpha, W)$ , discrete $W$ with $K < \infty$ atoms	$\sum_{v=1}^K \pi_{gv} \mathbf{1}_{\phi_v}$	Point mass at $\sum_{v=1}^K v \cdot \mathcal{I}(\theta = \phi_v)$
HDP	$\{1, \dots, K\}$	$\mathcal{W}_g(0, \alpha, W)$ , countably infinite $W$	$\sum_{v=1}^{\infty} \pi_{gv} \mathbf{1}_{\phi_v}$	$\mathbf{1}_{\{g\}}$ , prespecified $g \in \mathcal{G}$
PDP	$\{1\}$	$\mathcal{W}(d, \alpha, W)$	$\sum_{v=1}^{\infty} \pi_v \mathbf{1}_{\phi_v}$	$\mathbf{1}_{\{1\}}$
Dirichlet process	$\{1\}$	$\mathcal{W}(0, \alpha, W)$	$\sum_{v=1}^{\infty} \pi_v \mathbf{1}_{\phi_v}$	$\mathbf{1}_{\{1\}}$
Finite mixture	$\{1\}$	$\mathcal{W}(0, \alpha, W)$ , discrete $W$ with $K < \infty$ atoms	$\sum_{v=1}^K \pi_v \mathbf{1}_{\phi_v}$	$\mathbf{1}_{\{1\}}$

Table 1: Some examples of Sticky PDPs. Set  $\mathcal{N}$  represents the natural numbers. All the above examples correspond to singleton set  $\mathcal{S} = \{1\}$  and degenerate distribution  $\mathcal{Q}_g = \mathbf{1}_{\{1\}}$ . Refer to Section 2.1 for the notation.

In the MRF metaphor, there are two restaurants (i.e., groups), each serving two cuisines (i.e., states), with cuisine 1(2) representing non-differential (differential) state. Each cuisine consists of an infinite number of dishes (i.e.,  $T$ -variate latent vectors).

Property 2: The PDPs comprising the non-differential and differential states are modeled as follows.

**Non-differential state** Consider state (cuisine)  $s = 1$ , corresponding to the non-differential state. The two associated PDPs (restaurant–cuisine combinations) have the form

$$\mathcal{W}_{g1}(d_1, \alpha_1, W_1), \quad g = 1, 2. \quad (9)$$

Each  $T$ -variate latent vector in these PDPs has all equal elements because of non-differential state. That is, for positive integer  $v$ , latent vector  $\phi_v = \psi_v \mathbf{1}$ , where  $\psi_v \in \mathcal{R}$  and  $\mathbf{1}$  is the column vector of  $T$  ones. Since the  $\phi_v$  are iid draws from base distribution  $W_1$ , we have  $W_1 \stackrel{d}{=} \psi \mathbf{1}$ , where  $\psi \sim G$  for an unknown, univariate distribution  $G$ . In

order to be flexible, we assume that

$$G \sim \mathcal{DP}(\beta, G_0) \quad (10)$$

where  $\beta > 0$  is the mass parameter and  $G_0 = N(\mu_G, \tau_G^2)$  is the base distribution of the univariate Dirichlet process. Hyperparameters  $\mu_G$  and  $\tau_G^2$  are assigned conjugate priors.

The stick-breaking representation of the Dirichlet process implies that distribution  $G$  is almost surely discrete; specifically, it has the mass function

$$G(\psi) = \sum_{v=1}^{\infty} \varpi_v 1_{\zeta_v}(\psi), \quad \psi \in \mathcal{R}, \text{ where } \sum_{v=1}^{\infty} \varpi_v = 1 \text{ and } \zeta_v \stackrel{iid}{\sim} G_0. \quad (11)$$

The discreteness of  $G$  is critical because it results in base distribution  $W_1$  also being discrete, thereby allowing the two PDPs associated with non-differential state to choose from the same countable set of latent vectors. In the MRF metaphor, this allows the two restaurants to offer the same menu for cuisine 1. However, the allocation flexibility provided by PDPs is not important in the non-differential case because the allocation patterns of univariate real numbers are unidentifiable (e.g., see Frühwirth-Schnatter 2006). For this reason, we set PDP discount parameter  $d_1 = 0$ , reducing the PDPs in equation (9) to Dirichlet processes.

**Differential state** Now consider state (cuisine)  $s = 2$ , corresponding to the differential state. The associated PDPs (restaurant–cuisine 2 combinations) have the expression

$$\mathcal{W}_{g2}(d_2, \alpha_2, W_2), \quad g = 1, 2. \quad (12)$$

The multivariate base distribution  $W_2$ , from which the differential PDPs' latent vectors are drawn, must satisfy two conditions: (i) for all positive integers  $v$ , the latent vector

$\phi_v = (\phi_{1v}, \dots, \phi_{Tv})$  must have at least two unequal elements, and (ii) similar to the non-differential case, the base distribution should be discrete so that the two differential state PDPs share a countable set of latent vectors.

Using mass function  $G$  of equation (11), the mass function of a base distribution satisfying conditions (i) and (ii) may be constructed as follows. For every  $\phi = (\phi_1, \dots, \phi_T)'$ , let the mass function

$$W_2(\phi) = \begin{cases} \prod_{t=1}^T G(\phi_t) / (1 - \sum_{v=1}^{\infty} \varpi_v^T) & \text{if } \phi_t \neq \phi_{t'} \text{ for some } t \neq t', \\ 0 & \text{otherwise.} \end{cases} \quad (13)$$

Base distribution  $W_2$  is discrete because distribution  $G$  is discrete. The differential and non-differential states communicate through common distribution  $G$ , facilitating the borrowing of information across the states. Furthermore, the discreteness of distribution  $G$  results in additional dimension reduction in the differential latent vectors. This is an especially useful feature when the number of treatments,  $T$ , is large.

Unlike the non-differential situation, due to the special structure of mass function (13), in which  $T$ -dimensional latent vectors consist of exchangeable discrete components, the allocation patterns of the differential probe clusters become detectable with greater accuracy as  $T$  grows. For a detailed discussion of this remarkable phenomenon in the context of regular PDPs, refer to (Guha & Baladandayuthapani 2016, Section 4). For this reason, discount parameter  $d_2$ , controlling the allocation patterns, is given the mixture prior:

$$d_2 \sim \frac{1}{2}1_{\{0\}} + \frac{1}{2}U(0, 1) \quad (14)$$

where  $1_{\{0\}}$  denotes a point mass at 0. This allows the data to flexibly choose between a Dirichlet process and a more general PDP for a suitable clustering mechanism. For

example, probe allocation patterns that are characteristic of non-Dirichlet PDPs, such as power law decays in the cluster sizes and relatively large numbers of small-sized clusters, would cause posterior inferences for parameter  $d_2$  to exclude the value 0. On the other hand, allocation patterns that are more characteristic of Dirichlet processes, such as exponentially decaying cluster sizes dominated by a few large clusters, would result in high posterior probabilities being assigned to 0. A proof of the intrinsically different allocation patterns of Dirichlet processes and PDPs is given in (Guha & Baladandayuthapani 2016, Theorem 2.1).

Appropriate priors are assumed for the mass parameters,  $\alpha_1$ ,  $\alpha_2$  and  $\beta$ . Since base distribution  $W_2$  is discrete, the countable set of latent vectors shared by the two differential PDPs clusters, may possibly have repeats. In the MRF analogy, this corresponds to two tables in a restaurant section serving the same dish. Indeed, this is a common phenomenon when the number of treatments,  $T$ , is 2. However, the special structure of mass function (13) has another interesting consequence. Similar to the argument presented in (Guha & Baladandayuthapani 2016, Section 2.3), it can be shown that the probability of two latent vectors being identical rapidly decays to 0 as  $T$  grows, provided  $p$  grows at a slower-than-exponential rate as  $T$ . We have verified this in our simulations. For example, with  $p = 1,500$  probes, and with  $T$  as small as 4, we have not observed identical latent vectors associated with different PDP clusters in any of the artificial datasets that we have generated in our simulation studies.

Property 3: In general, let a realization of a PDP's stick-breaking distribution be denoted by  $\mathcal{P}_{gs}$ , where  $g, s = 1, 2$ . For probe  $j = 1, \dots, p$ , the label of the PDP generating random effect  $\boldsymbol{\theta}_j = (\theta_{1j}, \dots, \theta_{Tj})'$  is denoted by  $(g_j, s_j)$  where  $g_j, s_j \in \{1, 2\}$ . Consequently,  $\boldsymbol{\theta}_j \mid g_j, s_j \sim \mathcal{P}_{g_j s_j} \stackrel{d}{=} \sum_{v=1}^{\infty} \pi_{g_j s_j v} \mathbf{1}_{\phi_{g_j s_j v}}$ . Thus, for a positive integer  $v_j$  (representing the dish that customer  $j$  eats in the MRF analogy), random effect  $\boldsymbol{\theta}_j = \boldsymbol{\phi}_{g_j s_j v_j}$  with probability  $\pi_{g_j s_j v_j}$ .

Property 4: Given group  $g_j \in \{1, 2\}$  of the  $j^{th}$  probe, the state-specific PDP generating random effect  $\theta_j$  is distributed as  $s_j \mid g_j \sim \mathcal{Q}_{g_j}$ . Let parameter  $\rho \in (0, 1)$  be the *baseline differential proportion* and  $\rho' = 1 - \rho$  be the *baseline non-differential proportion*. For  $g, s = 1, 2$ , let mass function  $\mathcal{Q}_g(s)$  have the form

$$\mathcal{Q}_g(1) = \begin{cases} \rho' + \rho\gamma, & g = 1 \\ \rho' - \rho'\gamma, & g = 2 \end{cases} \quad (15)$$

and  $\mathcal{Q}_g(2) = 1 - \mathcal{Q}_g(1)$ , where  $0 < \gamma \leq 1$  is the *group purity parameter*. We assume independent uniform priors:  $\rho, \gamma \sim U(0, 1)$ . In other words, the non-differential and differential group respectively favors the non-differential and differential state relative to their baseline proportion. In the MRF analogy, each restaurant specializes in the cuisine having the same label, and the speciality cuisine is more popular there.

Property 5: For probe  $j > 1$ , group  $g_j$  has the distribution  $\mathcal{F}_{\theta_{j-1}, e_{j-1}}$ ; for the first probe,  $g_1 \sim \mathcal{F}_0(1) = \rho'$ . Let the scaled distance  $e_{j-1}$  between the  $(j-1)^{th}$  and  $j^{th}$  probes be transformed to an *affiliation* measure:

$$r_j = \exp(-e_{j-1}/\eta), \quad j > 1 \quad (16)$$

when the *range parameter*  $\eta > 0$ . When  $\eta = 0$ , we define affiliation  $r_j = 0$ . Thus,  $0 \leq r_j < 1$ .

The limiting value of  $\eta = 0$  corresponds to no dependence between any of the probes. Large values of  $\eta$  correspond to high serial dependencies that decrease with increasing inter-probe distances. Since the affiliation in equation (16) is unchanged when the distance  $e_{j-1}$  and parameter  $\eta$  are equally scaled, we may assume without loss of gen-

erality that the inter-probe distances  $e_1, \dots, e_{p-1}$  are scaled so that their sum equals 1. For example, if the probes represent biomarkers on a chromosome, then after scaling, the chromosome length is approximately equal to 1.

Recall that state  $s_{j-1}$  is a function of random effect  $\boldsymbol{\theta}_{j-1}$  because the PDP base distributions uniquely identify their states. Consequently, we assume that group  $g_j$  follows the distribution  $\mathcal{F}_{\boldsymbol{\theta}_{j-1}, e_{j-1}} = \mathcal{F}_{s_{j-1}, e_{j-1}}^*$  for some  $\mathcal{F}^*$ . In general, for every state  $s = 1, 2$ , scaled distance  $e \in (0, 1)$ , and affiliation  $r = \exp(-e/\eta)$ , we define the mass function of the groups as follows:

$$g \sim \mathcal{F}_{s,e}^*(1) = \begin{cases} \rho' + \rho r/\gamma, & s = 1 \\ \rho' - \rho' r/\gamma, & s = 2 \end{cases} \quad (17)$$

and  $\mathcal{F}_{s,e}^*(2) = 1 - \mathcal{F}_{s,e}^*(1)$ . For the mass function to be valid, it is necessary and sufficient that  $r/\gamma < 1$  for every  $0 < e < 1$ . Since  $e < 1$ , it can be verified that a sufficient condition is that  $\eta < -1/\log \gamma$ . Therefore, subject to this constraint, we assume the following mixture prior for  $\eta$  that lets the data decide whether to include dependence in the model:

$$\eta \mid \gamma \sim \frac{1}{2}1_{\{0\}} + \frac{1}{2}IG(1, \frac{1}{p-1}) \cdot \mathcal{I}(\eta < -1/\log \gamma)$$

The truncated inverse-gamma distribution follows from the constraint that, when the inter-probe distance  $e$  equals the sample mean distance of  $\sum_{j=2}^p e_{j-1}/(p-1) = 1/(p-1)$ , we obtain an objective (that is, uniform on its support) induced prior for affiliation  $r$ .

Equations (15) and (17) imply that

$$P(s_j = s \mid s_{j-1} = s) = \begin{cases} \rho' + \rho r_j, & s = 1 \\ \rho + \rho' r_j, & s = 2 \end{cases} \quad (18)$$

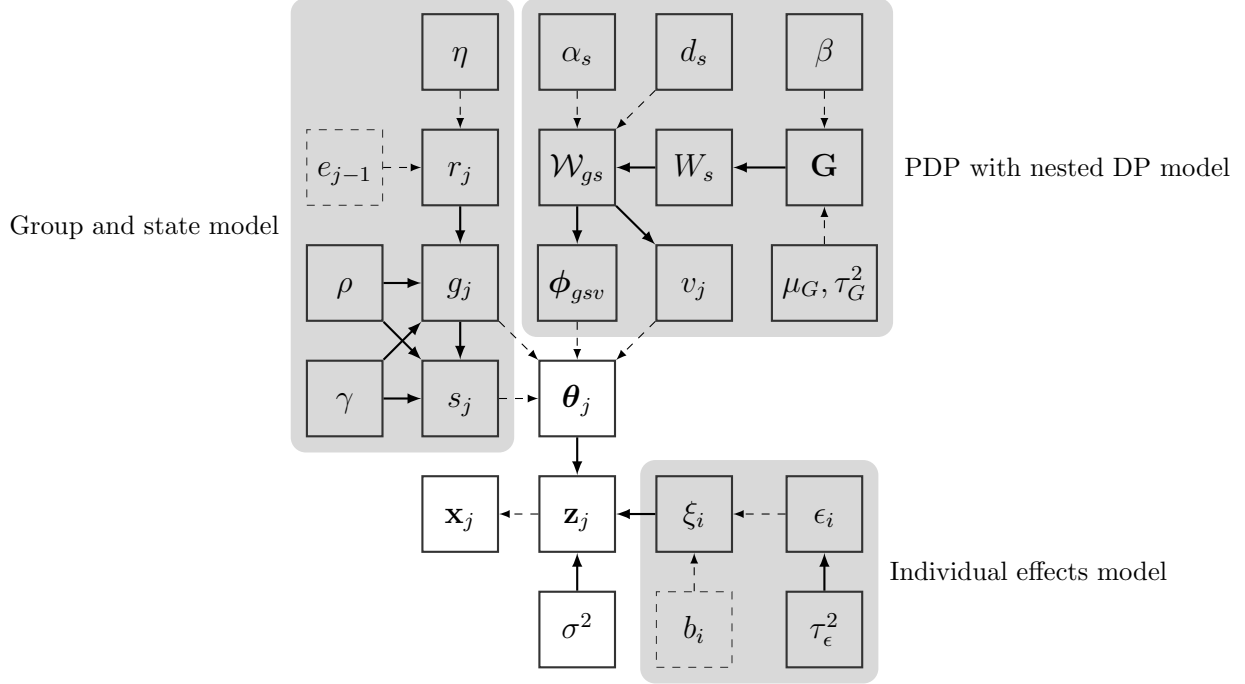


Figure 2: Directed acyclic graph of the BayesDiff model showing the relationship among the model components. Solid rectangles represent the data and model parameters; dashed rectangles represent predetermined model constants. Solid arrows represent stochastic relationships; dashed arrows represent deterministic relationships.

Relation (18) suggests that the next probe in the sequence has a relatively high probability of persisting in the same state as the previous probe, with the degree of persistence increasing with inter-probe affiliation (i.e., decreasing inter-probe distance). The usual case, where the differential state is relatively rare, corresponds to  $\rho < \rho'$  (i.e.,  $\rho < 1/2$ ), which implies from equation (18) that the persistence is lower for the differential state ( $s = 2$ ).

A directed acyclic graph illustrating the relationship among the BayesDiff model components is shown in Figure 2.

Finally, the general cluster allocation specified earlier in expression (4) can be linked to the afore-mentioned Sticky PDP clusters as follows. We inspect the group–state–cluster

labels actually allocated to the  $p$  probes. That is, we compute the set

$$\mathcal{C} = \left\{ (g_j, s_j, v_j) : j = 1, \dots, p \right\}$$

The number of distinct triplets belonging to the set  $\mathcal{C}$  equals the number of clusters,  $q$ , in expression (4). An arbitrary bijective mapping from the distinct triplets in set  $\mathcal{C}$  to the set  $\{1, \dots, q\}$  gives allocation variables  $c_1, \dots, c_p$  and the latent vectors  $\phi_1, \dots, \phi_q$  of expression (4).

### 3 Posterior Inferences

Due to the complexity of the proposed model, we apply MCMC methods to implement a fully Bayesian approach for posterior inference.

#### 3.1 Outline of the MCMC procedure

We iteratively update the model parameters by the following procedure:

1. Group variables  $g_1, \dots, g_p$ , state variables  $s_1, \dots, s_p$ , and cluster variables  $v_1, \dots, v_p$  are sequentially sampled given the remaining parameters. From their values, we compute the allocation variables  $c_1, \dots, c_p$  and the total number of PDP clusters,  $q$ .
2. The latent vectors  $\phi$ , consisting of  $Tq$  latent vector elements, are sampled conditional on the current probe cluster allocations and other model parameters. For  $s = 1, 2$ , let  $q_s$  be the total number of latent clusters allocated to the probes for PDPs associated with state  $s$ , irrespective of the groups. Since each latent vector in the non-differential PDPs clusters has just one unique element, this implies the number of distinct latent vector elements is  $(q_1 + Tq_2)$ . Due to the intensive nature of these Gibbs sampling updates, we apply the data squashing algorithm of Guha (2010) to speed up the computations.



3. Hyperparameters such as range parameter  $\eta$ , differential PDP discount parameter  $d_2$ , univariate Dirichlet process mass parameter  $\beta$ , base distribution hyperparameters, as well as other model parameters such as variance parameter  $\sigma^2$ , are sequentially sampled from their full conditional distributions via standard MCMC methods.

Further details are provided in the Supplementary Materials.

### 3.2 Detection of Differential Probes with FDR Control

The primary inferential goal is, of course, the detection of differential probes. For probe  $j$ , this information is encapsulated in the event  $[s_j = 2]$ . A Bayesian approach for controlling false discovery rate (FDR) (Newton et al. (2004)) is applied for detecting the differential probes.

Specifically, let  $q_0$  be the desired FDR level and  $\omega_j$  be the posterior probability of probe  $j$  being differential, so that  $\omega_j = P[s_j = 2 \mid \mathbf{X}]$ . An empirical average estimate,  $\hat{\omega}_j$ , is available from the MCMC sample. To achieve the desired FDR level in calling the differential probes, we first rank all the probes in decreasing order of  $\hat{\omega}_j$ . Let  $\hat{\omega}_{(1)} > \hat{\omega}_{(2)} > \cdots > \hat{\omega}_{(p)}$  denote the ordered posterior probability estimates. For each  $b = 1, \dots, p$ , we calculate the posterior expected FDR resulting from calling the first  $b$  probes in decreasing order of  $\hat{\omega}_j$ , as follows:

$$\widehat{\text{FDR}}_b = \frac{\sum_{j=1}^p (1 - \hat{\omega}_j) \mathcal{I}(\hat{\omega}_j \geq \hat{\omega}_{(b)})}{\sum_{j=1}^p \mathcal{I}(\hat{\omega}_j \geq \hat{\omega}_{(b)})} = \frac{\sum_{j=1}^b (1 - \hat{\omega}_{(j)})}{b} \quad (19)$$

where the simplified expression follows from the fact that the  $\hat{\omega}_j$ 's are sorted. Finally, we pick the largest value of  $b$ , denoted by  $b^*$ , for which  $\widehat{\text{FDR}}_{b^*} < q_0$ . The detection rule that labels as differential the first  $b^*$  probes, arranged in decreasing order of  $\hat{\omega}_j$ , achieves the desired FDR level.

## 4 Simulation Studies

To evaluate the ability of the BayesDiff procedure to detect the differential probes and learn the underlying dependence structure of the data, we analyzed artificially generated datasets with multiple treatments. The accuracy of BayesDiff was compared with those of some well-known differential methylation procedures and general statistical techniques for multigroup comparisons.

**Generation strategy** Continuous data were simulated from the Section 2 model with the identity transformation in equation (1), so that  $x_{ij} = z_{ij}$ . Since the offset  $b_i$  in equation (2) is known in applications, it was set equal to 0. The distances between the  $p$  probes were generated to mimic the actual distances in the colorectal cancer dataset, and were then scaled to sum to 1.

We considered four scenarios obtained by the combinations of two noise levels and two dependence levels. For each scenario, 20 datasets were generated, with each dataset consisting of  $p = 500$  probes and with  $T = 5$  treatments having 4 samples each, i.e.,  $n = 20$  samples. The low noise level corresponded to true variance parameter  $\sigma_0^2 = 0.64$ ; equivalently, true signal-to-noise ratio (SNR) of approximately  $R_0^2 = 0.7$ . The high noise level corresponded to true variance parameter  $\sigma_0^2 = 1.44$ ; equivalently, approximately  $R_0^2 = 0.4$ . The between-probe dependence had two levels: no serial correlation (i.e.,  $\eta_0 = 0$ ) and positive serial correlation of  $\eta_0 = 0.004$ . Although  $\eta_0 = 0.004$  may appear to be small, when the distance between two adjacent probes is equal to the average scaled distance of  $\bar{e} = 1/499$ , this value for  $\eta_0$  results in a true affiliation of 0.6 in equation (16). For convenience, we shall refer to the two dependence levels as “no correlation” and “high correlation,” respectively.

Other parameter values used to generate the datasets were common across the four scenarios. The values are displayed in Table 2. Each of the generated datasets contained about 10% differential probes. The data were then analyzed using the BayesDiff approach.

$\alpha_1$	$\alpha_2$	$d_2$	$\beta$	$\gamma$	$\rho$	$\mu_G$	$\tau_G^2$	$\tau_\epsilon^2$
20	20	0.33	20	0.9	0.1	0	1	0.1225

Table 2: Parameters used for data generation of simulation study

**Detecting the absence or presence of serial correlation** To assess the accuracy of BayesDiff in detecting the underlying dependence structure, depending on the true correlation level, we focused on the following log-Bayes factors. In the no-correlation (i.e.,  $\eta_0 = 0$ ) situation, we considered  $\log \left( \frac{P[\eta=0|\mathbf{X}]}{P[\eta>0|\mathbf{X}]} \right)$ . In the high correlation (i.e.,  $\eta_0 = 0.04$ ) situation, we considered  $\log \left( \frac{P[\eta>0|\mathbf{X}]}{P[\eta=0|\mathbf{X}]} \right)$ . Thus, in each situation, a large positive value for the corresponding log-Bayes factor would provide strong evidence that the correct correlation level was detected by BayesDiff.

Let  $\Theta^-$  denote all the model parameters except  $\eta$ . In the high correlation situation, applying Jensen’s inequality, a lower bound for the corresponding log-Bayes factor is found to be  $E \left[ \log \left( \frac{P[\eta>0|\mathbf{X}, \Theta^-]}{P[\eta=0|\mathbf{X}, \Theta^-]} \right) \mid \mathbf{X} \right]$ . Unlike log-Bayes factors, this lower bound can be estimated by an empirical average estimate computed from a single MCMC run. In the no correlation situation, a lower bound for the corresponding log-Bayes factor can be similarly derived. For each of the four generation scenarios, box plots of the estimated lower bounds for the 20 datasets are depicted in Figure 3.

The estimated lower bounds for the log-Bayes factors were all positive and sufficiently large. In the no correlation scenarios, BayesDiff favored zero order models. Although the estimates were smaller for the no correlation–high noise scenario, the smallest lower bound was 7.0, corresponding to Bayes factors exceeding  $e^{7.0} = 1,097$ . The 25<sup>th</sup> percentile of these lower bounds was 15.7, corresponding to Bayes factors exceeding  $e^{15.7} = 6,582,993$ . This is strong evidence that the BayesDiff approach is reliable in this scenario. For the high correlation scenarios, all the estimated lower bounds exceeded 50, corresponding to Bayes factors exceeding  $e^{50} = 5.18 \times 10^{21}$ . This shows that BayesDiff overwhelmingly favors first order models when the data are, in fact, spatially correlated.

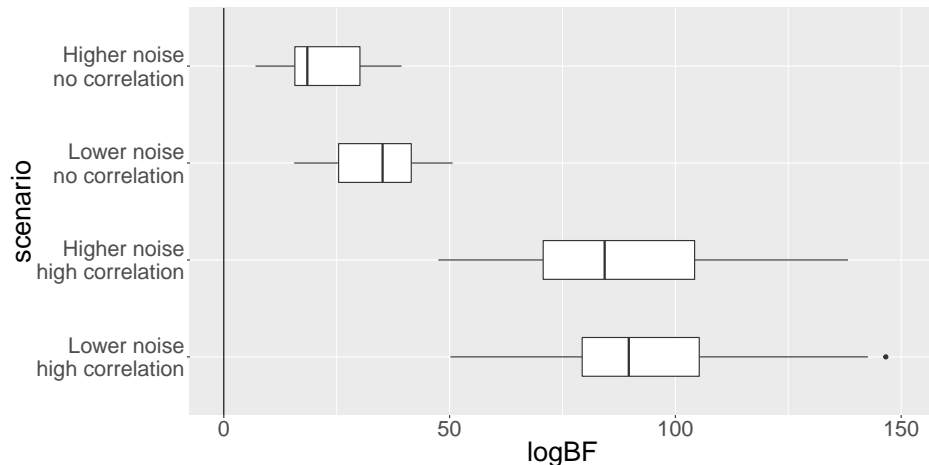


Figure 3: Box plots for the estimated lower bounds of the log-Bayes factors in favor of the true model order in artificial datasets.

**Comparisons with other methods** We evaluated the success of the BayesDiff procedure in detecting disease genomic signatures and made comparisons with six well-known procedures. These included general statistical techniques for multigroup comparisons, namely, one-way analysis of variance (ANOVA) and the Kruskal-Wallis test. We also made comparisons with some methods specially developed for detecting differential methylation in more than two treatments: COHCAP (Warden et al. 2013), methylKit (Akalin et al. 2012), BiSeq (Hebestreit et al. 2013), and RADMeth (Dolzhenko & Smith 2014).

The ANOVA and the Kruskal-Wallis test procedures were applied separately on each probe. For the methods designed for methylation datasets, we first converted the continuous values into proportions by applying the inverse-logit transformation. The transformed dataset was then analyzed by the COHCAP method. The remaining three methylation-related methods are designed for bisulfite sequencing, which consists of the total methylation reads for each measured CpG site. For these methods, we further assumed that there were 100 total reads for each probe, and so the methylation reads for each probe was obtained by multiplying the proportion methylation values by the total reads. The bandwidth smoothing parameter of the method BiSeq was tuned to optimize the overall detection. For all six

methods, the probe-specific p-values were obtained. The probes whose test p-values were less than the desired significance level were labeled as differential for that method.

We computed the receiver operating characteristic (ROC) curves for differential probe detection for all seven methods. The ROC curves, averaged over the 20 datasets under each simulation scenario, are shown in Figure 4; the individual ROC curves for each simulated datasets are available in Supplementary Materials. In all four scenarios, BayesDiff outperforms the other methods, as indicated by the fact that the areas below the ROC curves are greater for BayesDiff. As expected, all seven methods have lower accuracies for the higher noise levels. The performance of BayesDiff is significantly better than the competing methods in the high correlation scenarios, suggesting that the incorporation of between-probe dependencies greatly improves its accuracy. For a quantitative assessment, we calculated the area under curve (AUC) for the ROC curves, declaring the method as the most reliable when it has the largest AUC in a given scenario. In addition, since researchers typically focus on small false positive rates (FPRs), that is, small significance levels, we also calculated  $AUC_{20}$  and  $AUC_{10}$ .  $AUC_{20}$  ( $AUC_{10}$ ) is defined as the area under the ROC curve multiplied by 5 (10) when the FPR does not exceed 0.2 (0.1). The multiplicative factor ensures that the areas potentially vary between 0 and 1. The three versions of AUC are presented in Table 3.

Although BayesDiff uniformly has the largest AUC's in every scenario, it has vastly improved reliability for low FPRs. For example, consider the low noise-high correlation scenario. The overall AUC for BayesDiff is 0.073 higher than that for ANOVA. In contrast, the gains for BayesDiff, relative to ANOVA, are +0.201 for  $AUC_{20}$  and +0.276 for  $AUC_{10}$ . The relative advantages of BayesDiff are even greater for the other competing methods. This demonstrates that BayesDiff can accurately detect the differential probes even when the FPR is small.

## 5 Data Analysis

Returning to the motivating DNA methylation dataset, following the procedure proposed by Guinney et al. (2015), we classified the colorectal cancer samples into 4 consensus molecular subtypes (CMS), labeled CMS1, CMS2, CMS3, and CMS4. The 32 samples that were linked to no CMS were eliminated, leaving  $n = 131$  patient samples. We conducted the analysis on a gene-by-gene basis, picking a set of 499 genes that play a significant role in the classifier for the CMS groups. To ensure that all CpG sites that are potentially related to a gene are included in the analysis, we included all CpG sites within 250K base pair locations of the gene boundaries. The number of CpG sites included for each gene ranged from 13 to 1,137, and are displayed in Figure 5(a).

The data were analyzed using the proposed BayesDiff approach. Since DNA methylation data consist of proportions, the logit transformation was applied in expression (1). There are no known subject-specific offsets for this dataset, so the  $b_i$  values in expression (2) were set equal to 0. Appropriate priors were assigned to the model hyperparameters as described in Section 2. The data were analyzed using the MCMC procedure of Section 3.1. For detecting the differentially methylated CpG sites, we applied the Bayesian FDR control procedure of Section 3.2 after setting the desired FDR at  $q_0 = 0.05$ .

For each gene, Figure 5(b) displays 95% credible intervals for lower bounds of log-Bayes factors of a first versus zero order model, i.e.,  $\eta > 0$  in expression (16). Models with first order dependence are overwhelmingly favored for a majority of the genes, suggesting that methods that do not account for dependence between neighboring CpG sites would be less effective for these data.

Table 4 lists the genes containing at least 50% differentially methylated CpG sites. For these genes, the proportion of differentially methylated sites inside and outside the gene boundaries are also displayed. Although differential methylation is far more common inside the gene boundary for most of the genes, there are exceptions. Among the detected

differentially methylated sites, we estimated the pairwise differences between the random effects associated with the 4 CMS. For each gene, the CMS pair having the largest estimated difference in the majority of mapped CpG sites are listed in the last column of Table 4.

For most of the genes in Table 4, subgroup CMS1's higher methylation level relative to subgroup CMS2 is the largest pairwise difference. This makes sense because subgroup CMS1 is characterized by hypermethylation (Guinney et al. (2015)). However, it should be noted that three of the genes in the list (CCRL2, HOXD11, GRM8) exhibited lower methylation levels for subgroup CMS1. Further investigation of this finding is necessary in subsequent studies. For the top methylated genes, graphs with the detailed analysis results are displayed in Supplementary Materials. Although it is commonly believed that the CpG sites near 5' end is usually more important for differential methylation analysis, the 3' ends in some of the genes actually displayed more differential methylation.

Our findings both support and complement the known association between genes and colorectal cancer characteristics. For example, Fischer et al. (2001) found that stromal expression of gene COL5A2 is associated with malignancy in colorectal cancer. Pohl et al. (2015) pointed out that variation in expression level of gene SFRP4 contributes to the carcinogenesis of several cancers including colorectal cancer. Gene NCAM is known to function as a tumor suppressor for colorectal cancer (Roesler et al. (1997)). Loss in expression of gene DAB2 is found in colorectal cancer, among with several other types of cancer. Gene GPR155 is a potential early detection gene; for example, Shimizu et al. (2017) has shown that this gene predicts hematogenous metastasis in gastric cancer which, like colorectal cancer, belongs to the group of gastrointestinal (GI) cancers.

The high proportion of differentially methylated sites for these genes suggests that their methylation levels may also differentiate the CMS1 and CMS2 subgroups. Gains or losses of expression for a large variety of HOX genes have been reported in colorectal cancer (Abate-Shen (2002)). It is interesting that, in our analysis, the differential methylation in two members of this family of genes, HOXD11 and HOXC6, differentiate the subgroups CMS1

and CMS2, but in the opposite direction of their methylation levels.

## 6 Discussion

DNA methylation colorectal cancer data, like many other kinds of 'omics data, exhibit complex structures due to unknown biological mechanisms and distance-dependent serial correlations among neighboring CpG sites. The identification of the set of differentially methylated CpG sites on the epigenome is crucial for developing targeted treatments for the different subtypes of cancer. This paper formulates a flexible Bayesian approach applicable to DNA methylation datasets with multiple treatments called *BayesDiff*. The technique relies on a novel first order mixture model called the Sticky Poisson-Dirichlet process or the multicuisine restaurant franchise.

The success of the BayesDiff procedure in differential DNA methylation, relative to well-established strategies, is exhibited via simulation studies. We apply the new technique to detect the genomic signature for four subtypes of colorectal cancer in the motivating MD Anderson dataset. The data analysis result for colorectal cancer DNA methylation supports and complements various known features of differential methylation in cancer and associations between several genes and colorectal cancer. It also reveals a set of genes exhibiting high proportions of differential methylation among the cancer subtypes. These results emphasize the need for further investigation to better understand the biological mechanisms of the different subtypes of colorectal cancer.

Ongoing work involves extending the first order dependence in several types of datasets that necessitate incorporating more sophisticated forms of dependence. Equation (1) makes a platform-specific, deterministic global transformation and imposes a Gaussian mixture model on the transformed data. Due to the flexibility of Bayesian nonparametric models, this construction is likely to be adequate. However, we expect much greater dimension reduction in the large number of CpG sites by probabilistic frameworks such as the Conway-

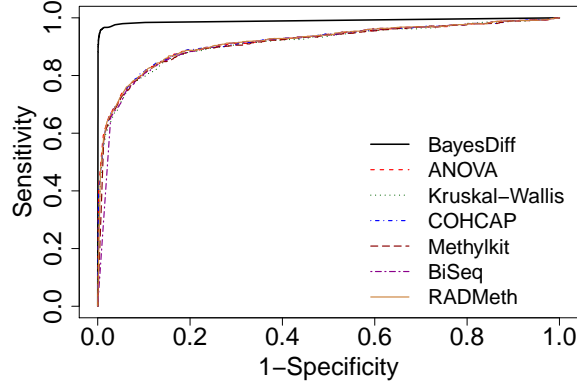


		Low noise		High noise	
		High correlation	No correlation	High correlation	No correlation
AUC	BayesDiff	<b>0.990</b>	<b>0.963</b>	<b>0.945</b>	<b>0.921</b>
	ANOVA	0.916	0.941	0.862	0.897
	Kruskal-Wallis	0.912	0.934	0.860	0.890
	COHCAP	0.916	0.940	0.861	0.895
	Methylkit	0.912	0.936	0.854	0.887
	BiSeq	0.910	0.932	0.857	0.891
	RADMeth	0.917	0.940	0.863	0.898
AUC <sub>20</sub>	BayesDiff	<b>0.977</b>	<b>0.910</b>	<b>0.883</b>	<b>0.797</b>
	ANOVA	0.776	0.821	0.614	0.697
	Kruskal-Wallis	0.758	0.800	0.599	0.672
	COHCAP	0.774	0.821	0.617	0.689
	Methylkit	0.756	0.802	0.600	0.667
	BiSeq	0.732	0.773	0.594	0.660
	RADMeth	0.769	0.816	0.613	0.692
AUC <sub>10</sub>	BayesDiff	<b>0.969</b>	<b>0.883</b>	<b>0.854</b>	<b>0.741</b>
	ANOVA	0.693	0.753	0.519	0.595
	Kruskal-Wallis	0.673	0.731	0.487	0.569
	COHCAP	0.686	0.753	0.518	0.580
	Methylkit	0.656	0.721	0.482	0.548
	BiSeq	0.608	0.661	0.469	0.536
	RADMeth	0.686	0.744	0.506	0.583

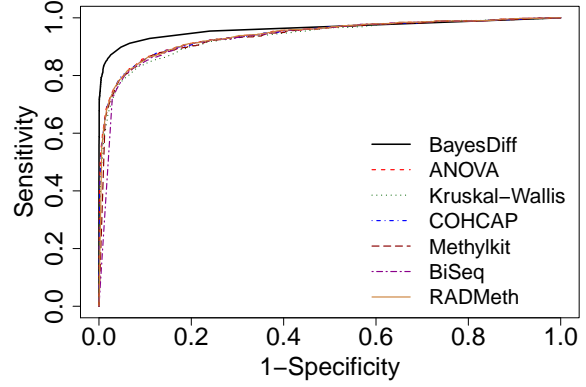
Table 3: Areas under ROC curves for the different methods (rows) under the four simulation scenarios (columns). See the text for further discussion.

Maxwell-Poisson distribution for overdispersed or underdispersed count data, logistic model for binary data, and probit model for proportion data. These extensions will be the focus of future papers.

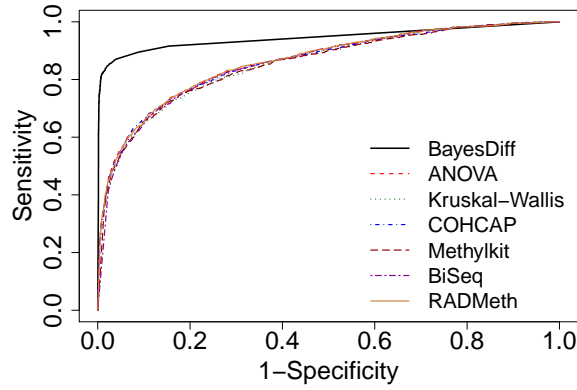
We are currently developing an R package implementing BayesDiff in a parallel computing framework using graphical processing units. The software will be made available for detecting genomic signatures in applications that extend beyond differential DNA methylation. Initial results indicate that dramatic speedups of several orders of magnitude would allow the analysis of user-specified datasets even on ordinary personal computers.



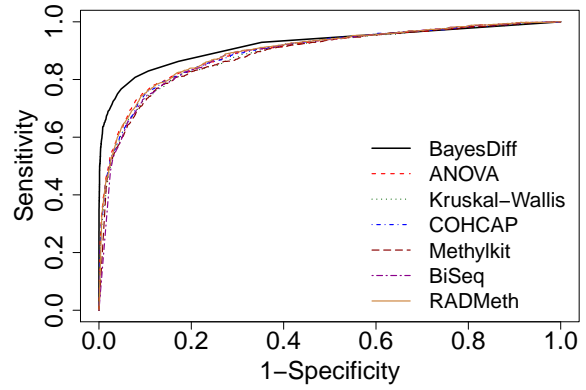
(a) Low noise, high correlation



(b) Low noise, no correlation



(c) High noise, high correlation

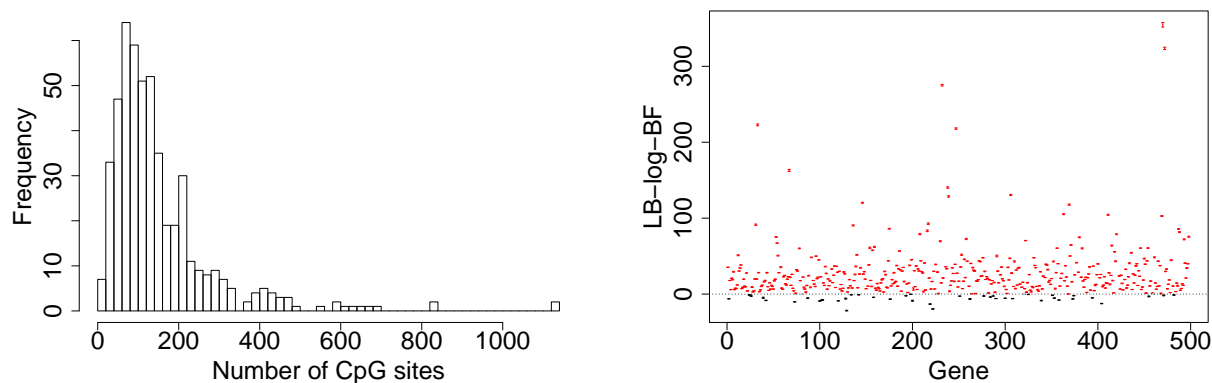


(d) High noise, no correlation

Figure 4: ROC curves, averaged over 20 simulated datasets, for the seven methods under the four simulation scenarios.

Gene name	Overall proportion	Total sites	Proportion inside	Sites inside	Proportion outside	Sites outside	Largest difference
COL5A2	0.61	36	0.36	11	0.72	25	CMS1↑ CMS2↓
TPSG1	0.60	826	1	5	0.60	821	CMS1↑ CMS2↓
SFRP4	0.56	55	0.58	12	0.56	43	CMS1↑ CMS2↓
TBC1D9	0.56	117	0.44	25	0.59	92	CMS1↑ CMS2↓
CCRL2	0.55	106	0.13	8	0.58	98	CMS2↑ CMS1↓
NCAM1	0.55	108	0.37	35	0.63	73	CMS1↑ CMS2↓
LDLRAD3	0.54	105	0.82	38	0.39	67	CMS2↑ CMS3↓
DAB2	0.54	48	0.46	13	0.57	35	CMS1↑ CMS2↓
TSHZ2	0.54	37	0.77	13	0.42	24	CMS1↑ CMS2↓
HOXD11	0.52	412	0.82	22	0.5	390	CMS2↑ CMS1↓
MEIS1	0.52	130	0.59	51	0.47	79	CMS2↑ CMS4↓
GRM8	0.51	72	0.76	38	0.24	34	CMS2↑ CMS1↓
ASCL2	0.50	609	0	11	0.51	598	CMS1↑ CMS2↓
HOXC6	0.50	458	0.52	31	0.50	427	CMS1↑ CMS2↓
GPR155	0.50	180	0.63	8	0.49	172	CMS1↑ CMS2↓
KCNJ8	0.50	76	0.57	7	0.49	69	CMS1↑ CMS2↓

Table 4: List of genes with at least 50% differentially methylated CpG sites, sorted in descending order. “Total sites” is the total number of CpG sites included for the gene. “Proportion inside (outside)” is the detected proportion of differentially methylated CpG sites inside (outside) the gene boundary. “Sites inside (outside)” is the total number of CpG sites inside (outside) the gene boundary. “Largest difference” indicates which pair-wise differences between the 4 CMS groups is the largest, with “↑ (↓)” representing higher (lower) methylation level for one CMS group compared to the other in the pair.



(a) Histogram of the number of gene-specific CpG sites (b) 95% credible intervals for lower bounds of log-Bayes factors of first order versus zero order models

Figure 5: Data analysis plots. See the text for further explanation.

## References

- Abate-Shen, C. (2002), ‘Deregulated homeobox gene expression in cancer: cause or consequence?’, *Nature reviews. Cancer* **2**(10), 777.
- Akalin, A., Kormaksson, M., Li, S., Garrett-Bakelman, F. E., Figueroa, M. E., Melnick, A. & Mason, C. E. (2012), ‘methykit: a comprehensive r package for the analysis of genome-wide dna methylation profiles’, *Genome biology* **13**(10), R87.
- Blei, D. M. & Jordan, M. I. (2005), ‘Variational inference for dirichlet process mixtures’, *Bayesian Analysis* **1**, 1–23.
- Dolzhenko, E. & Smith, A. D. (2014), ‘Using beta-binomial regression for high-precision differential methylation analysis in multifactor whole-genome bisulfite sequencing experiments’, *BMC bioinformatics* **15**(1), 215.
- Dunson, D. B., Herring, A. H. & Engel, S. M. (2008), ‘Bayesian selection and clustering of polymorphisms in functionally-related genes’, *Journal of the American Statistical Association* **103**, 534–546.
- Dunson, D. B. & Park, J.-H. (2008), ‘Kernel stick-breaking processes’, *Biometrika* **95**, 307–323.

- Eckhardt, F., Lewin, J., Cortese, R., Rakyan, V. K., Attwood, J., Burger, M., Burton, J., Cox, T. V., Davies, R., Down, T. A. et al. (2006), ‘Dna methylation profiling of human chromosomes 6, 20 and 22’, *Nature genetics* **38**(12), 1378.
- Feinberg, A. P. & Tycko, B. (2004), ‘The history of cancer epigenetics’, *Nature reviews. Cancer* **4**(2), 143.
- Feng, H., Conneely, K. N. & Wu, H. (2014), ‘A bayesian hierarchical model to detect differentially methylated loci from single nucleotide resolution sequencing data’, *Nucleic acids research* **42**(8), e69–e69.
- Ferguson, T. S. (1973), ‘A bayesian analysis of some nonparametric problems’, *The annals of statistics* pp. 209–230.
- Fischer, H., Stenling, R., Rubio, C. & Lindblom, A. (2001), ‘Colorectal carcinogenesis is associated with stromal expression of col11a1 and col5a2’, *Carcinogenesis* **22**(6), 875–878.
- Fox, E., Sudderth, E., Jordan, M. & Willsky, A. (2011), ‘The sticky hdp-hmm: Bayesian nonparametric hidden markov models with persistent states’, *Annals of Applied Statistics* **5**, 1020–1056.
- Frühwirth-Schnatter, S. (2006), *Finite Mixture and Markov Switching Models*, New York: Springer.
- Gnedin, A. & Pitman, J. (2005), ‘Regenerative composition structures’, *Annals of Probability* **33**, 445–479.
- Guha, S. (2010), ‘Posterior simulation in countable mixture models for large datasets’, *Journal of the American Statistical Association* **105**(490), 775–786.
- Guha, S. & Baladandayuthapani, V. (2016), ‘A nonparametric bayesian technique for high-dimensional regression’, *Electronic Journal of Statistics* **10**, 3374–3424.
- Guinney, J., Dienstmann, R., Wang, X., De Reyniès, A., Schlicker, A., Soneson, C., Marisa, L., Roepman, P., Nyamundanda, G., Angelino, P. et al. (2015), ‘The consensus molecular subtypes of colorectal cancer’, *Nature medicine* **21**(11), 1350–1356.
- Hamid, J. S., Hu, P., Roslin, N. M., Ling, V., Greenwood, C. M. T. & Beyene, J. (2009), ‘Data integration in genetics and genomics: methods and challenges’, *Human Genomics and Proteomics*.
- Hansen, K. D., Langmead, B. & Irizarry, R. A. (2012), ‘Bsmooth: from whole genome bisulfite sequencing reads to differentially methylated regions’, *Genome biology* **13**(10), R83.

- Hebestreit, K., Dugas, M. & Klein, H.-U. (2013), ‘Detection of significantly differentially methylated regions in targeted bisulfite sequencing data’, *Bioinformatics* **29**(13), 1647–1653.
- Irizarry, R. A., Ladd-Acosta, C., Carvalho, B., Wu, H., Brandenburg, S. A., Jeddeloh, J. A., Wen, B. & Feinberg, A. P. (2008), ‘Comprehensive high-throughput arrays for relative methylation (charm)’, *Genome research* **18**(5), 780–790.
- Irizarry, R. A., Ladd-Acosta, C., Wen, B., Wu, Z., Montano, C., Onyango, P., Cui, H., Gabo, K., Rongione, M., Webster, M. et al. (2009), ‘Genome-wide methylation analysis of human colon cancer reveals similar hypo-and hypermethylation at conserved tissue-specific cpg island shores’, *Nature genetics* **41**(2), 178.
- Jaffe, A. E., Murakami, P., Lee, H., Leek, J. T., Fallin, M. D., Feinberg, A. P. & Irizarry, R. A. (2012), ‘Bump hunting to identify differentially methylated regions in epigenetic epidemiology studies’, *International journal of epidemiology* **41**(1), 200–209.
- Kim, M. S., Lee, J. & Sidransky, D. (2010), ‘Dna methylation markers in colorectal cancer’, *Cancer and Metastasis Reviews* **29**(1), 181–206.
- Kim, S., Tadesse, M. G. & Vannucci, M. (2006), ‘Variable selection in clustering via dirichlet process mixture models’, *Biometrika* **93**, 877–893.
- Leek, J. T., Scharpf, R. B., Bravo, H. C., Simcha, D., Langmead, B., Johnson, W. E., Geman, D., Baggerly, K. & Irizarry, R. A. (2010), ‘Tackling the widespread and critical impact of batch effects in high-throughput data’, *Nature reviews. Genetics* **11**(10).
- Lijoi, A., Mena, R. & Prünster, I. (2007a), ‘Bayesian nonparametric estimation of the probability of discovering new species’, *Biometrika* **94**, 769–786.
- Lijoi, A., Mena, R. & Prünster, I. (2007b), ‘Controlling the reinforcement in bayesian non-parametric mixture models’, *Journal of the Royal Statistical Society: Series B (Statistical Methodology)* **69**, 715–740.
- Medvedovic, M., Yeung, K. Y. & Bumgarner, R. E. (2004), ‘Bayesian mixture model based clustering of replicated microarray data’, *Bioinformatics* **20**, 1222–1232.
- Müller, P. & Mitra, R. (2013), ‘Bayesian nonparametric inference—why and how’, *Bayesian analysis (Online)* **8**(2).
- Müller, P., Quintana, F. & Rosner, G. (2004), ‘A method for combining inference across related nonparametric bayesian models’, *Journal of the Royal Statistical Society, Series B* **66**, 735–749.

- Newton, M. A., Noueiry, A., Sarkar, D. & Ahlquist, P. (2004), ‘Detecting differential gene expression with a semiparametric hierarchical mixture method’, *Biostatistics* **5**(2), 155–176.
- Park, Y., Figueroa, M. E., Rozek, L. S. & Sartor, M. A. (2014), ‘Methylsig: a whole genome dna methylation analysis pipeline’, *Bioinformatics* **30**(17), 2414–2422.
- Perman, M., Pitman, J. & Yor, M. (1992), ‘Size-biased sampling of poisson point processes and excursions’, *Probability Theory and Related Fields* **92**(1), 21–39.
- Pohl, S., Scott, R., Arfuso, F., Perumal, V. & Dharmarajan, A. (2015), ‘Secreted frizzled-related protein 4 and its implications in cancer and apoptosis’, *Tumor Biology* **36**(1), 143–152.
- Rodriguez, A., B., D. D. & Gelfand, A. E. (2008), ‘The nested dirichlet process (with discussion)’, *Journal of the American Statistical Association* **103**, 1131–1144.
- Roesler, J., Srivatsan, E., Moatamed, F., Peters, J. & Livingston, E. H. (1997), ‘Tumor suppressor activity of neural cell adhesion molecule in colon carcinoma’, *The American journal of surgery* **174**(3), 251–257.
- Saito, Y., Tsuji, J. & Mituyama, T. (2014), ‘Bisulfighter: accurate detection of methylated cytosines and differentially methylated regions’, *Nucleic acids research* p. gkt1373.
- Shimizu, D., Kanda, M., Tanaka, H., Kobayashi, D., Tanaka, C., Hayashi, M., Iwata, N., Niwa, Y., Takami, H., Yamada, S. et al. (2017), ‘Gpr155 serves as a predictive biomarker for hematogenous metastasis in patients with gastric cancer’, *Scientific Reports* **7**.
- Siegel, R. L., Miller, K. D. & Jemal, A. (2017), ‘Cancer statistics, 2017’, *CA: A Cancer Journal for Clinicians* **67**(1), 7–30.
- Song, Q., Decato, B., Hong, E. E., Zhou, M., Fang, F., Qu, J., Garvin, T., Kessler, M., Zhou, J. & Smith, A. D. (2013), ‘A reference methylome database and analysis pipeline to facilitate integrative and comparative epigenomics’, *PloS one* **8**(12), e81148.
- Sun, D., Xi, Y., Rodriguez, B., Park, H. J., Tong, P., Meong, M., Goodell, M. A. & Li, W. (2014), ‘Moabs: model based analysis of bisulfite sequencing data’, *Genome biology* **15**(2), R38.
- Teh, Y. W., Jordan, M. I., Beal, M. J. & Blei, D. M. (2006), ‘Hierarchical dirichlet processes’, *J. Am. Statist. Ass.* **101**, 1566–1581.

- Tomlinson, G. & Escobar, M. (2003), ‘Analysis of densities’, *Talk given at the Joint Statistical Meeting* **103**, 1131–1144.
- Wang, D., Yan, L., Hu, Q., Sucheston, L. E., Higgins, M. J., Ambrosone, C. B., Johnson, C. S., Smiraglia, D. J. & Liu, S. (2012), ‘Ima: an r package for high-throughput analysis of illumina’s 450k infinium methylation data’, *Bioinformatics* **28**(5), 729–730.
- Warden, C. D., Lee, H., Tompkins, J. D., Li, X., Wang, C., Riggs, A. D., Yu, H., Jove, R. & Yuan, Y.-C. (2013), ‘Cohcap: an integrative genomic pipeline for single-nucleotide resolution dna methylation analysis’, *Nucleic acids research* **41**(11), e117–e117.
- Yu, X. & Sun, S. (2016), ‘Hmm-dm: identifying differentially methylated regions using a hidden markov model’, *Statistical applications in genetics and molecular biology* **15**(1), 69–81.